Distributions of tension and torsion in a threaded connection

Tengfei Shi[a], Yang Liu[b], Zhao Liu[a], Caishan Liu[a,*]

[a] *State Key Laboratory for Turbulence and Complex Systems, College of Engineering, Peking University, Beijing, 100871, China*

[b] *Exeter Small-Scale Robotics Lab, Engineering Department, University of Exeter, North Park Road, Exeter, EX4 4QF, UK*

Abstract

Threaded connection is a common structure in engineering applications, and its load distribution plays a critical role on the static and dynamic performances of the system. Although Sopwith (1948) studied the tension distribution along a thread helix, a model that includes the tension and torsion distributions in threaded connections is still missing. In this paper, we establish a comprehensive model which takes tension-torsion coupling into consideration for thread connection for the first time. In the proposed model, the bolt and nut are considered as two linearly elastic bodies with a tension-torsion coupling deformation, and deformation of the thread is calculated by the modified theory of the trapezoidal cantilever beam model. Based on the compatibility condition of these deformations, tension-torsion coupling equilibrium equations for the threaded connection can be built up. Our theoretical analysis shows that the proposed model agrees with the Sopwith's theory when the lead angle of the threaded connections is sufficiently small. However, the torque neglected by the Sopwith's theory must be taken into account in the cases of threaded connections with large lead angles. In addition, we perform a three-dimensional finite element analysis to demonstrate the validity of the proposed model. Finally, influence of geometrical and material parameters on load distribution is investigated. The finding of this work may provide a new insight into the fastening and anti-loosening design for threaded connections.

Keywords: Threaded connection ; Load distribution ; Tension-torsion coupling ; Analytical Model; FEM.

Nomenclature

β	Thread angle (°)
δ	Deflection of the thread ($\mathtt{m}$)
η	Lead angle (°)
η_c	Self-locked lead angle (°)
Γ	External torque ($\mathtt{N \cdot m}$)
δ_r	Relative deflection between threads ($\mathtt{m}$)
$\mathbf{F}$	Contact force between unit threads ($\mathtt{N/m}$)

*Corresponding author. e-mail: liucs@pku.edu.cn.

$\mathbf{R}_{fc}$ Transformation between Frenet and Cartesian Coordinates $(-)$

$\mathbf{R}_{fi}$ Transformation between Frenet and intermediate Coordinates $(-)$

$\mathbf{R}_{ic}$ Transformation between intermediate and Cartesian Coordinates $(-)$

$\mathbf{u}$ Total displacement of thread ($\mathtt{m}$)

$\mathbf{u}_r^f$ Tangential relative displacement between threads ($\mathtt{m}$)

$\mathbf{u}^s$ Thread displacement from main structure deformation ($\mathtt{m}$)

$\mathbf{u}^t$ Thread displacement from thread deformation ($\mathtt{m}$)

$\mathbf{w}_r^f$ Normal relative displacement between threads ($\mathtt{m}$)

μ Coefficient of friction between threads $(-)$

ω Governing parameter for axial load distribution ($\mathtt{1/m}$)

τ Torsional torque of per unit length ($\mathtt{N}$)

θ_b, θ_n Torsion displacements of bolt and nut (rad)

a, b, c Referenced helix parameters ($\mathtt{m}$)

A_b, A_n Cross-sectional areas of bolt and nut (m^2)

b, n Subscripts for bolt and nut $(-)$

d Width of thread root ($\mathtt{m}$)

d_m Width at midpoint of thread ($\mathtt{m}$)

E Young's modulus ($\mathtt{Pa}$)

E_rA_r Relative tensile stiffness between bolt and nut($\mathtt{N}$)

f^τ Tangential contact force between unit threads ($\mathtt{N/m}$)

f^n Normal contact force between unit threads ($\mathtt{N/m}$)

G Shear modulus ($\mathtt{Pa}$)

h Thread height ($\mathtt{m}$)

I_b, I_n Polar moment of inertias of nut's and bolt's cross-section($\mathtt{m}^4$)

k^n Normal stiffness of unit threads ($\mathtt{N/m}^2$)

k_r^n Tangential relative stiffness between unit threads ($\mathtt{N/m}^2$)

k_r^n Normal relative stiffness between unit threads ($\mathtt{N/m}^2$)

k_a Axial relative contact stiffness between threads($\mathtt{N/m}^2$)

L Engagement length between bolt and nut ($\mathtt{m}$)

La Thread lead ($\mathtt{m}$)

m Number of thread ($-$)

N_b, N_n Tension force of nut's and bolt's cross-section($\mathtt{N}$)

P External force ($\mathtt{N}$)

p Pitch of thread ($\mathtt{m}$)

q Axial contact force of per unit length ($\mathtt{N}/\mathtt{m}$)

r_b Radius of bolt ($\mathtt{m}$)

r_{ni} Inner radius of nut ($\mathtt{m}$)

r_{no} Out radius of nut ($\mathtt{m}$)

r_p Pitch radius of bolt and nut ($\mathtt{m}$)

s Arc-length of referenced helix ($\mathtt{m}$)

T_b, T_n Torsion torque of nut's and bolt's cross-section($\mathtt{N} \cdot \mathtt{m}$)

v Poisson's ratio ($-$)

w_b, w_n Tension displacements of bolt and nut (m)

x, y, z Position in Cartesian coordinate($\mathtt{m}$)

1. Introduction

Threaded connections are fundamental components in engineering applications for connecting[1–3], fastening[4–8], and sealing[9, 10]. They are widely used in civil, mechanical and biomedical engineering, see e.g. [11–19]. However, local mechanical behaviour of threaded connections could affect the overall static and dynamic performances of assembled structures significantly[20–26]. In order to achieve a good qualified design load distribution in threaded connections need to be studied thoroughly.

Building the mathematical model of a threaded connection is a challenging task due to the complex interactions between the threads in different geometric settings [27–29]. For the threaded connection that nut and bolt have an equal pitch, Hartog [30] found that bolt can be elongated and nut can be shortened under an axial tension load, causing the mating pitches no longer equal, so resulting in a nonuniform load distribution along the thread helix. An expression for the load distribution was derived by equating the sum of axial deformations of the bolt and nut to the deformation of the thread, which was treated as a cantilever beam subjected to bending action and the normal resultant force between threads was assumed to act on the midpoint of the cantilever beam. Later on, Sopwith [31] modified Hartog's model by taking into account Poisson's ratio on the radial compression of the thread and the radial displacement of the nut and bolt, which led to a succinctly theoretical model for load distribution. Thereafter, Yamamoto [32] developed a theoretical model for load distribution by modifying the thread contact stiffness, which considered the effects of inclination of the thread root, the shear deformation of the root, and the deformation due to radial extension and shrinkage. Recently, Lu et al. [33] extended the Yamamoto's model by including thread friction, and compared their theoretical results with finite element results. Goodier [34] used a bolt with a single turn of thread to study the load concentrations on different parts of the thread experimentally. The load distribution around the nut measured by extensometer measurements was consistent with Sopwith's theoretical results [31]. Kenny and Patterson [35] obtained the load distribution of an araldite bolt experimentally by using the photoelastic technique. They found a reasonable correlation between their experimental results and Sopwith's theory except for the loaded face of the nut. Such a discrepancy is due to the fact that the nut thread in the first pitch from the loaded face was not fully formed, and therefore exhibited a lower stiffness and load bearing capacity than a fully formed one [36]. Chen et al. [37] investigated the axial load distribution of a threaded connection using three dimensional photoelastic method, and their experimental results were consistent with the Sopwith's theory in general.

On the other hand, finite element methods (FEM) has been widely applied to study load distribution in threaded connections [38–40]. Due to the complex contact interactions between the threads of bolt and nut, many hypotheses were made in the FEM analysis of threaded connections [41]. In the early days of FEM development, researchers investigated load and stress distributions by using the non-threaded models, which ignored the influence of screw threads on load transfer. These approaches can capture the main mechanical characteristics of threaded connections while minimising the computational cost of FEM analysis. Maruyama [42] omitted the effect of friction and modelled the thread as annular grooves, thus approximating the problem of threaded connections to be axially symmetric. Maruyama's FEM results showed a good agreement with the experimental results obtained by using the copper-electroplating technique [43, 44]. In order to avoid the fine mesh of elements to the threads, Bretl and Cook [45] modelled the load transfer between a nut and a bolt by replacing the thread zone with a layer of elements having orthotropic properties. Segalman and Starr [46] presented a systematic method for representing the threaded volume by a continuous, homogeneous, linear elastic, anisotropic equivalent material. Motosh [47] divided the nut and bolt into a series of cylindrical elements and determined the load distribution of their threaded connection by using an iterative procedure. Wang and Marshek [48] developed a modified spring model for determining the load distribution in a threaded connection. Zhao [49] proposed a virtual contact loading method to study the load distributions in bolt-nut connectors. In order to reveal the stress in threads, axisymmetric FEM was used in the static analysis of threaded connections. In this case, threaded portions were modelled by negelecting the effects of lead angle and the helix of thread profile. Fukuoka et al. [50] performed a FEM analysis by using considering threaded connections as an axisymmetric problem. Furthermore, some researchers applied axisymmetric FEM models to perform elastoplastic stress and profile accuracy analyses for bolt-nut connections [51, 52]. In order to investigate the effect of friction and manufacturing accuracy investigation on the performance of the threaded connection, many researchers performed a 3D FEM analysis by considering the geometry of helical threads [53–56]. Some studies tried to elucidate the loosing phenomena of bolted joints by using the helical thread models [57–62], while some studies investigated the tightening process of threaded fasteners [63–65]. In addition, deformations in bolt-nut connection under thermal load can also be simulated by using 3D helical thread models [66–68].

Although Sopwith's theory can describe the load distribution of conventional threaded connections, there are still many hypotheses in the theory, leading to several ambiguities in the axial load relationship between each thread. Moreover, the Sopwith's model ignores the torsion deformation of bolt and nut, so it cannot be used for explaining the tightening and loosening mechanism of threaded fasteners. Until now, there are very few theoretical models that consider the tension-torsion coupling deformation in threaded connections. Although 3D FEM can obtain detailed information of stress concentration and contact pressure distribution, a trade-off between fine mesh and computational cost should be compromised [69]. Generally, in a threaded connection where both tension and torsion coexist, and for some engineering applications whose threads take large lead angles [70, 71], torsion load may have significant influence on the performance of threaded connections. In this case, both tension and torsion load must be considered in the analysis of threaded connections. Therefore, the present work aims to develop a new theoretical model for load distributions with the consideration of coupling of tensional and torsional deformations in threaded connections.

The contribution of this work is that the proposed model is more general and comprehensive compared to the Sopwith's theory (or Yamamoto's model) studied in [31–33]. In the present study, the main structures of bolt and nut were modelled as homogeneously elastic tension-torsion bars[72, 73], while threads were modelled as a continuous cantilever beam attached to the bolt and nut along the thread helix[33]. The load transfer between bolt's and nut's threads follow the modified cantilever beam theory in the Yamamoto's model, and the friction between the threads satisfied Coulomb's friction law. Through establishing the compatibility relationship between the deformations of bolt and nut and the deformations of contact threads, the tension-torsion coupled equations of equilibrium for the bolt and nut were then established. Combined with the boundary conditions of the bolt and nut, distributions of tensional and torsional loads were also obtained. The proposed model can be reduced to Sopwith's and Yamamoto's models when its lead angle is sufficiently small for which load distribution can be analytically expressed. Numerical results obtained from 3D FEM analysis were used to validate the proposed model. In addition, the influence of its geometrical and material parameters on load distribution was investigated thoroughly. In conclusion, the tension-torsion coupled model captures the stress distribution characteristic of threaded connection, and can be further used to study tightening process and anti-loosening of a bolt-nut connection.

The rest of this paper is organised as follows. Analysis for the deformations involved in bolt, nut and threads is carried out in Section 2. Section 3 presents the governing equations for a general bolt-nut connection . In Section 4, an analytical solution for the thread with a small lead angle is studied. In Section 5, the proposed model is validated by using FEM, and the influence of its physical parameters on load distribution is investigated. Finally, some conclusions are drawn in Section 6.

2. Deformation analysis of threaded connection

This section will present a detailed analysis for the deformation involved in a threaded connection. Firstly, the coordinates used for describing the geometries and deformations of the connection are introduced. Then Yamamoto's model will be used to calculate the contact stiffness of the thread, and the deformations of main structures of the bolt and nut will be defined. Finally, compatibility conditions for the deformations of the thread and the main structures will be established to describe the contact relationship between threads.

2.1. Description for threaded connection

Fig. 1 shows a bolt-nut connection, where a cylindrical bolt perfectly engages with a hollow-cylindrical nut through helical threads. The radius of the bolt is r_b, and the outer radius and inner radius of the nut are r_{no} and r_{ni}, respectively. Thus the pitch radius of the nut and bolt is $r_p = \frac{r_b + r_{ni}}{2}$. The pitch of the thread is p, and the number of thread is m, so the thread lead is given by $L_a = mp$. The length of the engagement between the bolt and nut is L. As shown in Fig. 1(c), the bolt and nut threads take the same isosceles-trapezoidal cross-section with the height h, root width d and thread angle β. The bolt and nut are made of materials with Young's modulus E_i, shear modulus G_i and Poisson's ratio ν_i, where the subscripts $i = b$ and n represent the bolt or nut, respectively. Finally, an external force P and a torque Γ are applied to the top end of the bolt along its axial direction.

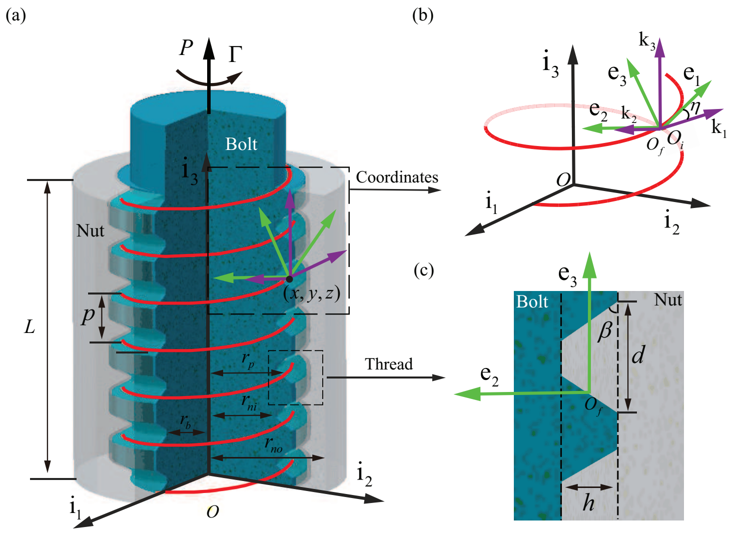

Figure 1: (Colour online) (a) A threaded connection consisting of a bolt with radius r_b and a nut with outer radius r_{no} and inner radius r_{ni}. The pitch of the thread is p and the pitch radius and the engagement of the connection are $r_p = \frac{r_b + r_{ni}}{2}$ and L, respectively. As shown by the red line, a referenced helix with radius of curvature r_p representing the geometric centre of the engaging faces between the threads are defined to investigate the contact relationship between the bolt and nut. (b) A Cartesian coordinate $(O - \mathbf{i}_1\mathbf{i}_2\mathbf{i}_3)$ is located at the bottom center of the bolt. And at any point on the referenced helix, a local Frenet coordinate $(O_f - \mathbf{e}_1\mathbf{e}_2\mathbf{e}_3)$ and an intermediate coordinate $(O_i - \mathbf{k}_1\mathbf{k}_2\mathbf{k}_3)$ are defined. (c) A detailed cross-sectional view of the trapezoid thread with height h, root width d and thread angle β.

Let us define a Cartesian coordinate $(O - \mathbf{i}_1\mathbf{i}_2\mathbf{i}_3)$ with origin O at the bottom of the bolt and $\mathbf{i_3}$ along the axis of the bolt. To investigate the contact relationship between the bolt thread and nut thread, we need to define a referenced helix with radius of curvature r_p, representing the geometric centre of the engaging faces between the bolt's and nut's threads before deformation. We assume that this referenced helix is invariable after a small elastic deformation. The referenced helix can be parameterised using the arc-length s, whose original point, $s = 0$, is located at $(r_p, 0, 0)$ in the coordinate $(O - \mathbf{i}_1\mathbf{i}_2\mathbf{i}_3)$. Thus, any point on the referenced helix can be described in the Cartesian coordinate as

$$\begin{cases} x(s) = a\cos\frac{s}{c}, \\ y(s) = a\sin\frac{s}{c}, \\ z(s) = b\frac{s}{c}, \end{cases} \tag{1}$$

where

$$\begin{cases} a = r_p, \\ b = \frac{L_a}{2\pi}, \\ c = \sqrt{a^2 + b^2}. \end{cases} \tag{2}$$

At any point on the referenced helix, a local Frenet coordinate $(O_f - \mathbf{e}_1\mathbf{e}_2\mathbf{e}_3)$ is defined as shown in Fig. 1(b), where $\mathbf{e}_1$, $\mathbf{e}_2$ and $\mathbf{e}_3$ are the tangential, normal and binormal vectors, respectively. In addition, the plane $(O_f - \mathbf{e}_2\mathbf{e}_3)$ corresponds to the cross-section of the thread as shown in Fig. 1(c). Here, we introduce an intermediate coordinate $(O_i - \mathbf{k}_1\mathbf{k}_2\mathbf{k}_3)$ generated by rotating the coordinate $(O_f - \mathbf{e}_1\mathbf{e}_2\mathbf{e}_3)$ around $\mathbf{e}_2$ with a lead angle η. The relationship between the lead angle and referenced helix parameters are

$$\begin{cases} \sin\eta = \frac{b}{c}, \\ \cos\eta = \frac{a}{c}, \\ \tan\eta = \frac{b}{a}. \end{cases} \tag{3}$$

Clearly, $\mathbf{k}_2$ and $\mathbf{k}_3$ are parallel to $\mathbf{e}_2$ and $\mathbf{i}_3$, respectively. The coordinate transformation matrix among the Cartesian coordinate $(O - \mathbf{i}_1\mathbf{i}_2\mathbf{i}_3)$, the Frenet coordinate $(O_f - \mathbf{e}_1\mathbf{e}_2\mathbf{e}_3)$ and the intermediate coordinate $(O_i - \mathbf{k}_1\mathbf{k}_2\mathbf{k}_3)$ are given as

$$\begin{bmatrix} \mathbf{e}_1 \\ \mathbf{e}_2 \\ \mathbf{e}_3 \end{bmatrix} = \mathbf{R}_{fi} \begin{bmatrix} \mathbf{k}_1 \\ \mathbf{k}_2 \\ \mathbf{k}_3 \end{bmatrix} = \mathbf{R}_{fi}\mathbf{P}_{ic} \begin{bmatrix} \mathbf{i}_1 \\ \mathbf{i}_2 \\ \mathbf{i}_3 \end{bmatrix} = \mathbf{R}_{fc} \begin{bmatrix} \mathbf{i}_1 \\ \mathbf{i}_2 \\ \mathbf{i}_3 \end{bmatrix}, \tag{4}$$

where $\mathbf{R}_{fc} = \mathbf{R}_{fi}\mathbf{R}_{ic}$ and

$$\mathbf{R}_{fi} = \begin{bmatrix} \frac{a}{c} & 0 & \frac{b}{c} \\ 0 & 1 & 0 \\ -\frac{b}{c} & 0 & \frac{a}{c} \end{bmatrix}, \mathbf{R}_{ic} = \begin{bmatrix} -\sin\frac{s}{c} & -\cos\frac{s}{c} & 0 \\ \cos\frac{s}{c} & -\sin\frac{s}{c} & 0 \\ 0 & 0 & 1 \end{bmatrix}, \mathbf{R}_{fc} = \begin{bmatrix} -\frac{a}{c}\sin\frac{s}{c} & -\frac{a}{c}\cos\frac{s}{c} & \frac{b}{c} \\ \cos\frac{s}{c} & -\sin\frac{s}{c} & 0 \\ \frac{b}{c}\sin\frac{s}{c} & \frac{b}{c}\cos\frac{s}{c} & \frac{a}{c} \end{bmatrix}. \tag{5}$$

2.2. Thread deflection and its contact stiffness

To investigate the deformation of the thread, as shown in Fig. 2, the screw thread can be modeled as a short cantilever beam with the thickness being the length of the thread helix, and contact force between threads can be simplified as a resultant force. In order to determine the location of the resultant force, Nassar[8] simplified the complex normal contact force between threads was uniformly distributed or linearly distributed along radial direction. The FEM results of Liu et. al [62] showed that the normal contact force was neither uniform distributed nor linear distributed, but the resultant forces was located near the midpoint of the thread.

Assuming the normal resultant force acts at the midpoint of the thread and taking thread's bending, radial compression and the Poisson ratio effect into consideration, Sopwith [31] built up a modified theory for symmetric triangle cantilever beam model to calculate the equivalent contact stiffness that links the normal force to the deflection at the midpoint of the thread. Based on Sopwiths theory, Yamamoto [32] and Lu et al. [33] simplified the thread as a trapezoidal cantilever beam and considered more factors to calculate the contact stiffness more precisely. In this paper, we use Yamamoto's model to compute the contact stiffness of the thread.

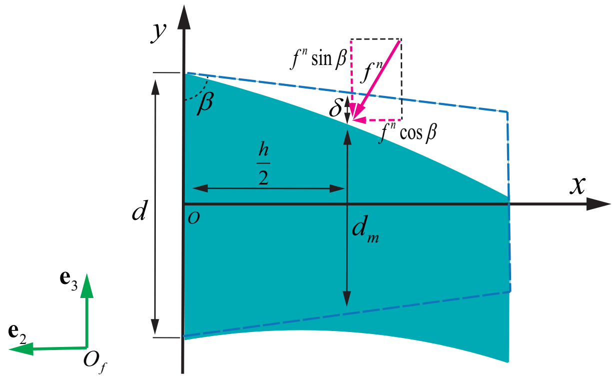

Figure 2: (Colour online) Total deflection δ of a thread under normal contact pressure which is assumed to be uniformly distributed and can be simplified as an equivalent normal contact force at the midpoint of the thread in $(O_f - \mathbf{e_2}, \mathbf{e_3})$ plane.

Fig. 2 shows the cross-sectional shape of the thread before and after deformation, where f^n represents the resultant force per unit length of the thread helix, acting at midpoint along the normal direction of bearing face of the thread. The cross-section is located on the $O_f - \mathbf{e}_2\mathbf{e}_3$ plane, and takes an isosceles-trapezoid shape with the height h, root width d and thread angle β. Thus, the width at midpoint is given by $d_m = d - 2h\cot\beta$. The deflections at the midpoint of the thread due to different factors are illustrated in Fig. 3, where $\delta_{1,j}$, $\delta_{2,j}$, $\delta_{3,j}$ and $\delta_{4,j}$ represent the deflections along $\mathbf{e}_3$ direction induced by thread's bending, shearing, the incline at the thread root and the shear at the thread root, respectively. Here, $j = b$ or n stands for bolt or nut, respectively.

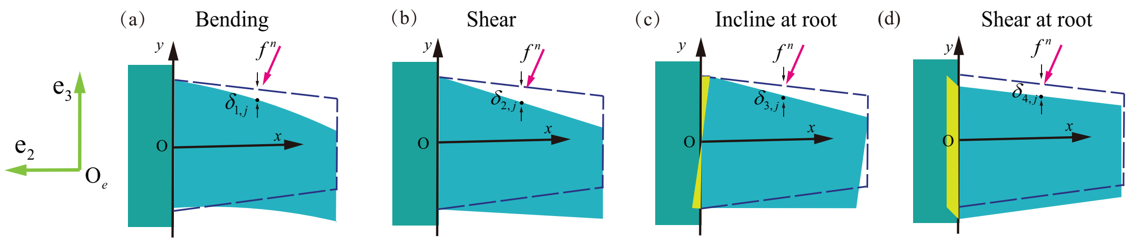

Figure 3: (Colour online) Deflections of the thread induced by (a) thread's bending, (b) shearing, (c) the incline at the thread root and (d) the shear at the thread root, where $j = b$ or n stands for bolt or nut, respectively.

According to [32, 33], the relationship between the normal force f^n and the deflections $\delta_{1,j}$, $\delta_{2,j}$, $\delta_{3,j}$ and $\delta_{4,j}$ are given by

$$\begin{cases} \delta_{1,j} &= \frac{3\sin\beta(1-\nu_j^2)}{4E_j}\left\{\left[1-\left(2-\frac{d_m}{d}\right)^2+2\ln\left(\frac{d}{d_m}\right)\right]\frac{1}{\cot^3\beta}-4\left(\frac{h}{2d}\right)^2\cot\beta\right\}f^n, \\ \delta_{2,j} &= \frac{6\sin\beta(1+\nu_j)}{5E_j\cot\beta}\ln\left(\frac{d}{d_m}\right)f^n, \\ \delta_{3,j} &= \frac{6\sin\beta(1-\nu_j^2)h}{\pi E_j d^2}\left(\frac{h}{2}-\frac{d_m}{2}\cot\beta\right)f^n, \\ \delta_{4,j} &= \frac{2\sin\beta(1-\nu_j^2)}{\pi E_j}\left[\frac{p}{d}\ln\left(\frac{p+d/2}{p-d/2}\right)+\frac{1}{2}\ln\left(4\frac{p^2}{d^2}-1\right)\right]f^n, \end{cases} \tag{6}$$

In addition, Yamamoto [32] introduced a correction term considering the deflection caused by the radial contraction and expansion of the bolt and nut, respectively. This is given by

$$\delta_{5,j} = \begin{cases} \frac{\sin\beta(1-\nu_b)\cot^2\beta r_b}{2pE_b} f^n & \text{for } \ j=b, \\ \frac{\sin\beta\cot^2\beta r_{ni}}{2pE_n}\left(\frac{r_{no}^2+r_{ni}^2}{r_{no}^2-r_{ni}^2}+\nu_n\right) f^n & \text{for } \ j=n. \end{cases} \tag{7}$$

Combing all the deflections together, the total deflection along $\mathbf{e}_3$ direction of the thread for the bolt and nut can be calculated as $\delta_j = \sum_{i=1}^{5}\delta_{i,j}$. According to Eqs. (6) and (7), it is clear that the deformation depends on the load f^n linearly. Therefore, the equivalent contact stiffness of the thread can be computed as

$$k_j^n = \frac{f^n}{\delta_j}, \tag{8}$$

which depends on the geometry and material properties of the thread.

As shown in Fig. 2, Yamamoto's model considers the deflection along the binormal direction $\mathbf{e}_3$ only. The shear deformation of the thread along $\mathbf{e}_1$ and the compression deformation of the thread along $\mathbf{e}_2$ are small enough to be ignorable. Therefore, the displacements of threads of the bolt and nut at their midpoint induced by the thread interaction can be written in the Frenet Coordinate $(O_i - \mathbf{e}_1\mathbf{e}_2\mathbf{e}_3)$ as

$$\begin{cases} \mathbf{u}_b^t = \delta_b\mathbf{e}_3, \\ \mathbf{u}_n^t = \delta_n\mathbf{e}_3. \end{cases} \tag{9}$$

2.3. Deformation field of the bolt and nut

To model the bolt-nut connection, deformations in the structure must be considered. Here, both bolt and nut that are subjected to tension and torsion deformations only are modelled as homogeneous elastic bars with the uniform cross-sections , $A_b = \pi r_b^2$ and $A_n = \pi(r_{no}^2 - r_{ni}^2)$, respectively. Fig. 4 shows a description for the deformation fields of the threaded connection, where the tension deformations of the bolt and nut are determined by the translational displacements $w_b(z)$ and $w_n(z)$, respectively, and their torsion deformations are modelled by the angular displacements , $\theta_b(z)$ and $\theta_n(z)$. Under the homogeneity assumption, $w_b(z)$, $w_n(z)$, $\theta_b(z)$ and $\theta_n(z)$ are the functions with respect to the Cartesian axis, z.

As shown in Fig. 4(a), define B_b and B_n are the midpoint points of the bolt's and nut's threads, respectively, which are a pair of engaging points located in the reference helix curve. Due to the deformations of the main structures, these two coincident points will take certain elastic displacements. Here, we use $\mathbf{u}_b^s(z)$ and $\mathbf{u}_n^s(z)$ to denote these two displacements of B_b and B_n. As shown in Fig. 4(b), the coordinate components of $\mathbf{u}_b^s(z)$ and $\mathbf{u}_n^s(z)$ in the intermediate coordinate $(O_i - \mathbf{k}_1\mathbf{k}_2\mathbf{k}_3)$ can be written as

$$\begin{cases} \mathbf{u}_b^s(z) = b\theta_b(z)\mathbf{k}_1 + w_b(z)\mathbf{k}_3, \\ \mathbf{u}_n^s(z) = b\theta_n(z)\mathbf{k}_1 + w_n(z)\mathbf{k}_3. \end{cases} \tag{10}$$

Using the transformations in Eq. (4), $\mathbf{u}_b^s(z)$ and $\mathbf{u}_n^s(z)$ in the Frenet coordinate $(O_f - \mathbf{e}_1\mathbf{e}_2\mathbf{e}_3)$ are given

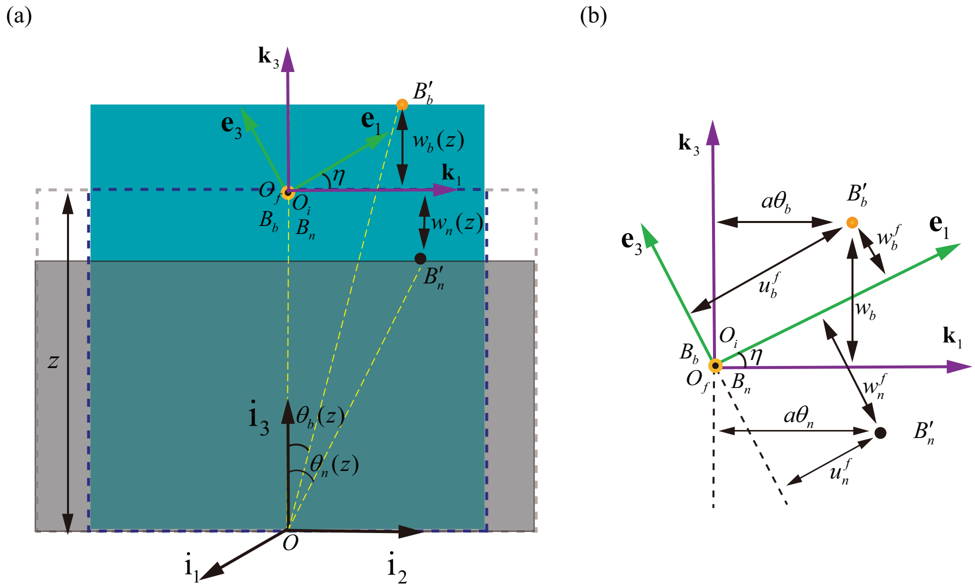

Figure 4: (Colour online) (a) The bolt and nut are modeled as bending-torsional coupling elastic bars. The dashed rectangle and the solid rectangle are the outlines of the bolt and nut before and after deformation, respectively. bolt's tension deformation , bolt's torsion deformation , nut's tension deformation and nut's torsion deformation are denoted by w_b, w_b, w_n and w_n, respectively. (b) Before deformation, a pair of engaged points B_b and B_n on the bolt's and nut's threads, respectively, are located at the origins of $(O_i - \mathbf{e}_1\mathbf{e}_2\mathbf{e}_3)$ and the intermediate coordinate $(O_i - \mathbf{k}_1\mathbf{k}_2\mathbf{k}_3)$. Due to the tensional and torsional deformations of the bolt and nut, B_b and B_n will move to B_b' and B_n', respectively.

by

$$\begin{cases} \mathbf{u}_b^s(z) & = u_b^f(z)\mathbf{e}_1 + w_b^f(z)\mathbf{e}_3 \\ & = \left[\frac{b}{c}w_b(z) + \frac{a^2}{c}\theta_b(z)\right]\mathbf{e}_1 + \left[\frac{a}{c}w_b(z) + \frac{ab}{c}\theta_b(z)\right]\mathbf{e}_3, \\ \mathbf{u}_n^s(z) & = u_n^f(z)\mathbf{e}_1 + w_n^f(z)\mathbf{e}_3 \\ & = \left[\frac{b}{c}w_n(z) + \frac{a^2}{c}\theta_n(z)\right]\mathbf{e}_1 + \left[\frac{a}{c}w_n(z) + \frac{ab}{c}\theta_n(z)\right]\mathbf{e}_3. \end{cases} \tag{11}$$

2.4. Compatibility condition for thread contact

Let $\mathbf{u}_b$ and $\mathbf{u}_n$ be the total displacements of thread's midpoint of the bolt and nut, respectively. According to Eqs.(9) and (11), the total displacements can be written in the Frenet coordinate $(O_f - \mathbf{e}_1\mathbf{e}_2\mathbf{e}_3)$ as

$$\begin{cases} \mathbf{u}_b = \mathbf{u}_b^t + \mathbf{u}_b^s = u_b^f\mathbf{e}_1 + (w_b^f + \delta_b)\mathbf{e}_3, \\ \mathbf{u}_n = \mathbf{u}_n^t + \mathbf{u}_n^s = u_n^f\mathbf{e}_1 + (w_n^f + \delta_n)\mathbf{e}_3. \end{cases} \tag{12}$$

Based on the non-penetration condition between contacting bodies, the two engaged contact points $\{B_b, B_n\}$ should take the same elastic displacements along the binormal direction $\mathbf{e}_3$, i.e., $w_b^f + \delta_b = w_n^f + \delta_n$, which can be rewritten as

$$\delta_r = -w_r^f, \tag{13}$$

where $\delta_r = \delta_b - \delta_n$ and $w_r^f = w_b^f - w_n^f$ are the relative deflection and the normal relative translation between the bolt and nut threads, respectively. Alone the tangential direction $\mathbf{e}_1$, the contact pair

$\{B_b, B_n\}$ will have a relative displacement

$$\mathbf{u}_r^f = u_r^f \mathbf{e}_1 = (u_b^f - u_n^f)\mathbf{e}_1. \tag{14}$$

Substituting Eq. (11) into Eqs. (13) and (14) gives the compatibility conditions for a thread contact

$$\begin{cases} \delta_r & = -w_r^f \\ & = -\frac{a}{c}(w_b - w_n) + \frac{ab}{c}(\theta_b - \theta_n), \\ u_r^f & = \frac{b}{c}(w_b - w_n) + \frac{a^2}{c}(\theta_b - \theta_n), \end{cases} \tag{15}$$

which describes the normal relative deflection and the tangential relative displacement between a pair of engaged threads as functions of the tension and torsion deformations of the main structures of the bolt and nut.

3. Governing equations for the bolt-nut connection

This section will establish the governing equations for the bolt-nut connection. Firstly, the derivations of the thread contact force by the contact constitutive relation and the compatibility condition are presented. Then the differential equilibrium equations considering the tension and torsion of the bolt-nut connection are established. Finally, some boundary conditions are presented.

3.1. Contact force between threads

According to Eq. (8), we can describe the relationship between the normal contact force f^n per unit arc-length and the deflection of the bolt thread as

$$\delta_b = \frac{f^n}{k_b^n},$$

where k_b^n is the normal stiffness of the bolt thread. Similarly, the thread deflection of the nut subjected to the reaction force is given by

$$\delta_n = \frac{-f^n}{k_n^n},$$

where k_n^n is the normal stiffness of the nut thread. Thus, the relative deflection between the bolt and nut threads can be calculated as

$$\delta_r = \delta_b - \delta_n = f^n \tfrac{k_b^n + k_n^n}{k_b^n k_n^n},$$

which can be rewritten as

$$f^n = k_r^n \delta_r, \tag{16}$$

where $\delta_r = \delta_b - \delta_n$ and $k_r^n = \frac{k_b^n k_n^n}{k_b^n + k_n^n}$.

In the tangential direction $\mathbf{e}_1$, the tangential relative displacement $\mathbf{u}_r^f$ in Eq. (14) will cause a friction force $\mathbf{f}^\tau = f^\tau \mathbf{e}_1$ between the threads of the bolt and nut. Introducing a tangential relative contact stiffness k_r^τ, and considering the Coulomb friction law, the tangential contact force can be obtained as

$$f^\tau = \begin{cases} -k_r^\tau \mathbf{u}_r^f & \text{if} \quad \left|k_r^\tau u_r^f\right| < \mu \left|f^n\right|, \\ -\mu \left|f^n\right| \frac{\mathbf{u}_r^f}{\left|\mathbf{u}_r^f\right|} & \text{if} \quad \left|k_r^\tau u_r^f\right| \geq \mu \left|f^n\right|. \end{cases} \tag{17}$$

where μ is the coefficient of friction between the threads.

Substitution of the compatibility condition in Eq. (15) into the constitutive relations in Eqs. (16) and (17) gives

$$\begin{cases} f^n = -k_r^n \left[\frac{a}{c}(w_b - w_n) - \frac{ab}{c}(\theta_b - \theta_n)\right], \\ f^\tau = \begin{cases} -k_r^\tau \left[\frac{b}{c}(w_b - w_n) + \frac{a^2}{c}(\theta_b - \theta_n)\right] & \text{if } \left|k_r^\tau u_r^f\right| < \mu \left|f^n\right|, \\ -\mu \left|f^n\right| \frac{\mathbf{u}_r^f}{\left|\mathbf{u}_r^f\right|} & \text{if } \left|k_r^\tau u_r^f\right| \geq \mu \left|f^n\right|, \end{cases} \end{cases} \tag{18}$$

which describe the normal and tangent contact force between the threads as functions of the tension and torsion displacements of the main structures of bolt and nut.

According to the geometry of the thread illustrated in Fig. 2, the contact force $\mathbf{F^f}$ applied on a small segment of the bolt thread having a length ds can be expressed in the Frenet coordinate as

$$\begin{aligned} \mathbf{F^f} &= F_1^f \mathbf{e}_1 + F_2^f \mathbf{e}_2 + F_3^f \mathbf{e}_3 \\ &= f^\tau \mathrm{d}s\mathbf{e}_1 + f^n \cos\beta \mathrm{d}s\mathbf{e}_2 + f^n \sin\beta \mathrm{d}s\mathbf{e}_3. \end{aligned} \tag{19}$$

Using the coordinate transformation shown in Eq. (4), the contact force in an arc-length ds can be rewritten in the Cartesian coordinate as

$$\begin{aligned} \mathbf{F} &= \mathbf{F^f}\mathbf{P_{fc}} \\ &= F_1\mathbf{i_1} + F_2\mathbf{i_2} + F_3\mathbf{i_3} \\ &= \left[-\frac{a}{c}F_1^f \sin\left(\frac{s}{c}\right) - F_2^f \cos\left(\frac{s}{c}\right) + \frac{b}{c}F_3^f \sin\left(\frac{s}{c}\right)\right]\mathbf{i_1} \\ &\quad + \left[\frac{a}{c}F_1^f \cos\left(\frac{s}{c}\right) - F_2^f \sin\left(\frac{s}{c}\right) - \frac{b}{c}F_3^f \cos\left(\frac{s}{c}\right)\right]\mathbf{i_2} \\ &\quad + \left[\frac{b}{c}F_1^f + \frac{a}{c}F_3^f\right]\mathbf{i_3}. \end{aligned} \tag{20}$$

As shown in Eq. (1), the arc-length s and the axial length z follows $s = \frac{c}{b}z$, so, d$s = \frac{c}{b}$dz. Considering a bolt connection with the thread number m, the axial force $q(z)$ per unit axial length of the contact force $\mathbf{F}$ along $\mathbf{i_3}$ can then be written as

$$q(z) = m\frac{F_3}{dz} = mf^\tau + m\frac{a}{b}f^n \sin\beta. \tag{21}$$

The torsional torque $\tau(z)$ generated from the contact force $\mathbf{F}$ per unit axial length along $\mathbf{i_3}$ can then be given by

$$\begin{aligned} \tau(z) &= (\mathbf{r}_{OO_f} \times \frac{\mathbf{F}}{dz}) \cdot \mathbf{i_3} \\ &= m\left[\frac{F_2}{dz}a\cos\left(\frac{s}{c}\right) - \frac{F_1}{dz}a\sin\left(\frac{s}{c}\right)\right] \\ &= m\frac{a^2}{b}f^\tau - maf^n \sin\beta. \end{aligned} \tag{22}$$

Substituting Eq. (18) into Eq. (21) and (22), it is clear that the axial contact distributed force $q(z)$ and the distributed torque $\tau(z)$ are functions of the tension and torsion deformations. We can write them in a general form as follows,

$$\begin{cases} q & = q(w_b,\ \theta_b,\ w_n,\ \theta_n), \\ \tau & = \tau(w_b,\ \theta_b,\ w_n,\ \theta_n). \end{cases} \tag{23}$$

3.2. Equations of equilibrium

As the main structures of bolt and nut are simplified as homogeneous elastic bars, their constitutive relationship can be expressed as

$$\begin{cases} N_i = E_i A_i \frac{\mathrm{d}w_i}{\mathrm{d}z}, \\ T_i = G_i I_i \frac{\mathrm{d}\theta_i}{\mathrm{d}z}, \end{cases} \tag{24}$$

where A_i and I_i are the area and the polar moment of inertia of the nut's or bolt's cross-section, respectively. N_i and T_i represent the tension force and the torque applied on the section located at position z, respectively.

Along the axial direction, the bolt is subjected to a distributed axial load $q(z)$ and a distributed torque $\tau(z)$ generated by the interaction between the threads of the bolt and nut. As shown in Fig. 5, we analyse an infinitesimal segment with a length $\mathrm{d}z$, the balance equations of the infinitesimal segment can be written as

$$\begin{cases} \mathrm{d}N_b + q(z)\mathrm{d}z = 0, \\ \mathrm{d}T_b + \tau(z)dz = 0. \end{cases} \tag{25}$$

Similarly, the nut along its axial direction is subjected to the reaction axial force and the reaction torque. Therefore, the balance equations for an infinitesimal segment of the nut can be written as

$$\begin{cases} \mathrm{d}N_n - q(z)\mathrm{d}z = 0, \\ \mathrm{d}T_n - \tau(z)\mathrm{d}z = 0. \end{cases} \tag{26}$$

Considering Eqs. (23) and (24), the tensional and torsional differential equations of equilibrium for the main structures of bolt and nut can be written as

$$\begin{cases} E_b A_b \frac{\mathrm{d}^2 w_b}{\mathrm{d}z^2} + q(w_b,\ \theta_b,\ w_n,\ \theta_n) = 0, \\ E_n A_n \frac{\mathrm{d}^2 w_n}{\mathrm{d}z^2} - q(w_b,\ \theta_b,\ w_n,\ \theta_n) = 0, \\ G_b I_b \frac{\mathrm{d}^2 \theta_b}{\mathrm{d}z^2} + \tau(w_b,\ \theta_b,\ w_n,\ \theta_n) = 0, \\ G_n I_n \frac{\mathrm{d}^2 \theta_n}{\mathrm{d}z^2} - \tau(w_b,\ \theta_b,\ w_n,\ \theta_n) = 0. \end{cases} \tag{27}$$

Once the boundary conditions of the bolt connection are given, we can numerically solve or theoretically analyse Eq. (27) to obtain the deformation field of the bolt and nut.

3.3. Boundary conditions

Depending on the loading environment, different boundary conditions can be assigned for the bolt-nut connection. Here, we consider a specific situation where the nut is fixed while the bolt is subjected to an external tension and torque. In this case, the nut takes a fixed boundary at the bearing surface $z = L$

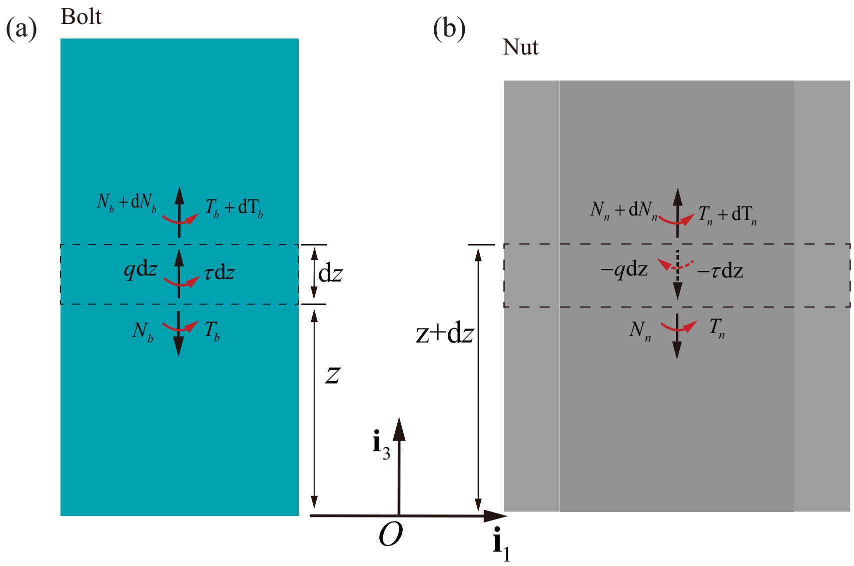

Figure 5: (Colour online) Equilibrium of an infinitesimal element for (a) bolt and (b) nut .

while the surface at $z = 0$ has no external load. The boundary conditions of the nut can then be expressed as

$$\begin{cases} \left.\frac{\mathrm{d}w_n}{\mathrm{d}z}\right|_{z=0} = 0, \quad w_n|_{z=L} = 0, \\ \left.\frac{\mathrm{d}\theta_n}{\mathrm{d}z}\right|_{z=0} = 0, \quad \theta_n|_{z=L} = 0. \end{cases} \tag{28}$$

At the surface $z = L$ of the bolt, there are external tension P and torque Γ representing the internal load of the bolt, respectively. The surface at $z = 0$ can be considered as a free surface. Therefore, the boundary conditions for the bolt are given by

$$\begin{cases} \left.\frac{\mathrm{d}w_b}{\mathrm{d}z}\right|_{z=0} = 0, \quad \left.E_bA_b\frac{\mathrm{d}w_b}{\mathrm{d}z}\right|_{z=L} = P, \\ \left.\frac{\mathrm{d}\theta_b}{\mathrm{d}z}\right|_{z=0} = 0, \quad \left.E_bA_b\frac{\mathrm{d}\theta_b}{\mathrm{d}z}\right|_{z=L} = \Gamma, \end{cases} \tag{29}$$

By using the boundary equations Eqs. (28) and (29), the coupled equations in Eq. (27) can be calculated to obtain the distributions of tension and torsion in the bolt-nut connection.

4. Analytical solution for small lead angle under tension

For the bolt-nut connection under the condition that nut is fixed and bolt is only subjected to an external tension force, the connection may be self-locked due to friction if the lead angle is sufficiently small. When no external torque is applied on the bolt, the total torque induced by the friction should be equal to zero, namely, $\int \tau(z)dz = 0$. At the critical state of Coulomb friction, we have $f^\tau = \mu f^n$ and the direction of $\tau(z)$ should be identical. This means that we must have $\tau = 0$. Accordingly, we can get from Eq. (22) the maximum lead angle η_c responsible for a self-locked connection,

$$\eta_c = \arctan\left(\frac{\mu}{\sin\beta}\right). \tag{30}$$

Clearly, the self-locked lead angle increases as the thread angle β decreases. This is the reason why the trapezoid thread is often used for static connection, while the rectangle thread is used for screw translation.

For the bolt-nut connection with a small lead angle, i.e., $\eta < \eta_c$, we can assume that the static friction torque generated by the threads take the same direction when the bolt is only subjected to an axial load. So the equality $\tau = 0$ still exists. In this case, from Eq. (22) the static friction force can be expressed as $f^\tau = \frac{b}{a} f^n \sin\beta$. Substituting this relationship into Eq. (21) gives

$$q = m\tfrac{c^2}{ab} f^n \sin\beta, \tag{31}$$

where the geometrical relationship in the third term of Eq. (2) is used.

Noting that $\tau = 0$ means that no torsional deformation is generated when the bolt is only subjected to an axial load. Namely, we have $\theta(z)_n = \theta_b(z) \equiv 0$. Thus, substituting the first term of Eq. (18) into the Eq. (31) leads to the relationship between the axial load distribution q and the tension deformations of the main structures of the bolt and nut,

$$q = -\tfrac{mk_r^n \sin\beta}{\sin\eta}(w_b - w_n) = -k_a(w_b - w_n), \tag{32}$$

where Eq. (3) is used, and $k_a = \frac{mk_r^n \sin\beta}{\sin\eta}$ can be considered as the axial relative contact stiffness between the threads.

By subtracting the first two equations of Eq. (27), we get

$$E_r A_r \tfrac{\mathrm{d}^2 q}{\mathrm{d}z^2} = k_a q, \tag{33}$$

where $E_r A_r = \frac{E_b A_b E_n A_n}{(E_b A_b + E_n A_n)}$ is the relative tensile stiffness between the bolt and nut. Combining Eqs. (32) and (33), the governing equation for the distribution of the contact force between the threads is given by

$$\tfrac{\mathrm{d}^2 q}{\mathrm{d}z^2} - \omega^2 q = 0, \tag{34}$$

where

$$\omega = \sqrt{\tfrac{k_a}{E_r A_r}} = \sqrt{\tfrac{mk_r^n \sin\beta}{E_r A_r \sin\eta}}. \tag{35}$$

The governing equation Eq. (34) has an identical form with the governing equation in Sopwith's and Yamamoto's modes [31, 32]. However, the governing parameter ω in Eq. (34) has a clearer physical meaning.

The general solution of Eq. (34) is

$$q = \psi_1 e^{\omega z} + \psi_2 e^{-\omega z}, \tag{36}$$

where ψ_1 and ψ_2 are integration constants to be determined by the boundary conditions.

In order to determine ψ_1 and ψ_2, we can use the boundary conditions given by Eqs. (28) and (29). For the free cross-section at $z = 0$, the corresponding condition related to q can be expressed as

$$\left.\tfrac{\mathrm{d}q}{\mathrm{d}z}\right|_{z=0} = -k_a \left.\tfrac{\mathrm{d}(w_b - w_n)}{\mathrm{d}z}\right|_{z=0} = 0. \tag{37}$$

Besides, the integration of the contact force along the whole engagement should be balanced with the external tensile force, which can be expressed as

$$\int_0^L q \mathrm{d}z = P. \tag{38}$$

Substituting Eq. (36) into Eqs. (37) and (38), the integration constants are determined as $\psi_1 = \psi_2 = \frac{P\omega}{e^{\omega L} - e\omega^{-\omega L}}$. Then the exact solution of Eq. (36) can be written as

$$q = \frac{P\omega}{e^{\omega L} - e^{-\omega L}} \left(e^{\omega z} + e^{-\omega z} \right). \tag{39}$$

In Eq. (39), it can be seen that the distribution of the contact force is mainly affected by ωL . When $\omega L \gg 1$, the terms $e^{-\omega z}$ can be neglected, so Eq. (39) can be simplified as

$$q = \frac{F\omega}{e^{\omega L}} e^{\omega z}, \tag{40}$$

leading to an exponential distribution for the axial load along the axial direction, where the closer to the load surface, the greater the axial load.

When $\omega L \ll 1$, by using the Taylor expansion $e^{\omega z} = 1 + \omega z + O(\omega^2 z^2)$, the solution of Eq. (39) can be rewritten as

$$q = \frac{P}{L}. \tag{41}$$

In this case, the contact force seems to uniformly distributes along the axial direction. Clearly, the dimensionless quantity ωL is a key parameter to influence the distribution of the contact force.

If the lead angle of the bolt-nut connection is greater than the maximum self-locked lead angle, i.e., $\eta > \eta_c$, either a fixed boundary condition or an external torque should be assigned at $z = L$ for maintaining the connection balance. If a fixed boundary at z=L is assigned, Eq. (29) should be changed as

$$\begin{cases} \left.\frac{\mathrm{d}w_b}{\mathrm{d}z}\right|_{z=0} = 0, \quad E_b A_b \left.\frac{\mathrm{d}w_b}{\mathrm{d}z}\right|_{z=L} = F. \\ \left.\frac{\mathrm{d}\theta_b}{\mathrm{d}z}\right|_{z=0} = 0, \quad \theta_b|_{z=L} = 0. \end{cases} \tag{42}$$

In this case, the condition $\tau = 0$ is no longer kept, and the torsional deformations must be considered in the modeling. Therefore, we must solve the coupled equations in Eq. (27) combined with the boundary conditions in Eqs. (28) and (42). The coupling makes the analytical solution having complex expressions that can not be expressed as a simple form as the case of the thread connection with a small lead angle. In the following section, we will present numerical solution to demonstrate how the coupling affects the load distribution.

5. Numerical investigations

5.1. Parameters of the bolt-nut connection

In the following simulations, two cases of bolt-nut connections are studied, where one case is for small lead connection whose lead angle is smaller than its the maximum self-locked lead angle, while the other one is for the lead angle bigger than its the maximum self-locked lead angle.

The parameters of the bolt-nut connections are listed in Table 1. For the case of the connection with a small lead angle, the pith is $p = 3$ mm, and the number of the thread is $m = 1$, so $L_a = mp = 3$ mm. We assign the large lead angle connection with pith $p = 4$ mm, $m = 3$, so $L_a = mp = 12$ mm. The cross-section of the thread for the small lead case is trapezoidal with $d = 2.65$ mm, $h = 2.00$ mm and $\beta = 60°$, while the cross-section of the thread for the large lead case is rectangular with $d = 1.47$ mm, $h = 2.00$ mm and $\beta = 90°$. For both cases, the radii of the bolt and nut are $r_b = 9$ mm, $r_{ni} = 11$ mm and$r_{no} = 15$ mm, and the engaged length between the bolt and nut is $L = 24$ mm. The Young's modulus of elasticity and the Poisson's ratio of the bolt and nut in both cases are the same. In addition, the relative tangential contact stiffness is $k_r^{\tau} = 6.5 \times 10^9$ N/m^2 which is obtained by empirical fitting, and the friction between the bolt and nut is set as $\mu = 0.1$.

Parameters	Small lead	Large lead	Unit
Pitch, p	3	3	mm
Thread number, m	1	4	–
Lead, L_a	3	12	mm
Thread hight, h	2	2	mm
Thread width, d	2.65	1.47	mm
Thread angle, β	60	90	$\circ$
Thread friction, μ	0.1	0.1	–
Bolt radius, r_b	9	9	mm
Nut inner radius, r_{ni}	11	11	mm
Nut outer radius, r_{no}	15	15	mm
Engaged length, L	24	24	mm
Young's modulu, E	2×10^{11}	2×10^{11}	Pa
Poisson's ratio, v	0.3	0.3	–
Tangential stiffness, k_r^{τ}	6.5×10^9	6.5×10^9	N/m^2

Table 1: Physical parameters of the bolt-nut connections.

In terms of Eqs. (2), (3) and (30), together with the parameters shown in Table 1, we can obtain $\eta = 1.7°$ and $\eta_c = 6.6°$ for the small lead case, while $\eta = 6.8°$ and $\eta_c = 5.7°$ for the large lead case. Noting that $\eta < \eta_c$ for the small lead case, we can find its theoretical solution for tension load distribution according to Eq. (39) and the torque $\tau = 0$ when the bolt-nut connection is only subjected to an external axial load P. For the large lead case, we have $\eta > \eta_c$. In this case, no theoretical solution can be found, and a fixed boundary should be assigned at $z = L$ for balance, even though the bolt-nut connection is only subjected to an external axial load P. In the following, we will perform FEM analysis for verifying the above discussions.

5.2. Model validation via finite element method

To validate the proposed bolt-nut connection model, two finite element (FE) models for the small and large lead cases were developed by using ANSYS WORKBENCH. Fig. 6 shows the two FEM models, in which the geometrical and material parameters in Table 1 were adopted. The quadratic tetrahedron element with 10 nodes (Solid 187) was selected to discretise the bolt and nut, and the element sizes of the main structure and the thread are limited less than 1 mm and 0.2 mm, respectively. The contact interaction between the threads of the bolt and nut was modelled by using frictional face-to-face elements. According the boundary conditions for the small lead case as shown in Eqs. (28) and (29) , both the cross-section of the bolt and the nut at $z = 0$ is set to free, while the cross-section of the bolt and the nut at $z = L$ is applied to an external force P and external torque Γ along z and is fixed, respectively.

For the large lead case, cross-sections of the bolt and the nut at $z = 0$ are also free, and cross-section of the nut at $z = L$ is fixed. However, the rotation of cross-section of the bolt at $z = L$ is limited and is only applied an external force P along z, which is corresponding to Eq. (42). After solving the FE models, we can employe the probe tool in the post-processor of the FEM software to obtain the tension and torsion distribution along the axial direction of the connection.

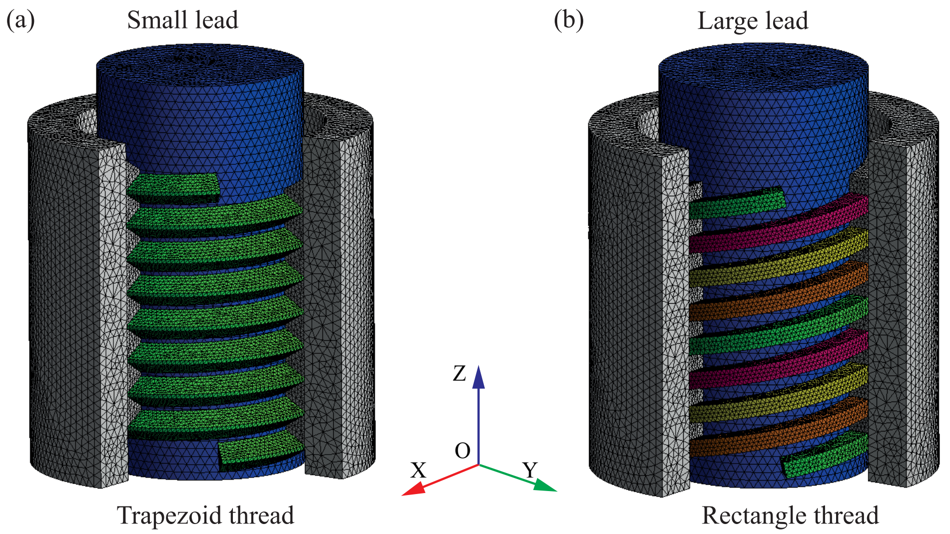

Figure 6: (Colour online) Finite element models of the bolt-nut connections for (a) the small lead case with 1 trapezoid thread and (b) the large lead case with 4 rectangle threads. The quadratic tetrahedron element with 10 nodes was selected to discretise the connections, and the element sizes of the main structure and the thread are limited less than 1 mm and 0.2 mm, respectively. The contact interaction between the threads was modelled by using frictional face-to-face elements. Both bolt and nut are shown by a three-quarters view.

To numerically solve the tension-torsion coupled equation Eq. (27) under the boundary conditions as shown in Eqs. (28), (42) and (42), the Euler difference technique [74, 75] was employed. Both the bot and nut were divided into $(\kappa - 1)$ identical pieces with κ nodal points. Besides, a dummy point was added outside both ends of the nut and bolt to calculate derivations of the end nodal points. Through the discretisation, the displacement of the connection can be written as $\mathbf{X} = [\mathbf{w}_b, \boldsymbol{\theta}_b, \mathbf{w}_n, \boldsymbol{\theta}_n]^{\mathrm{T}} \in \mathbb{R}^{4(\kappa+2)}$, where $\mathbf{w}_b = [w_b^0, w_b^1 \cdots, w_b^{\kappa+1}]$, $\boldsymbol{\theta}_b = [\theta_b^0, \theta_b^1 \cdots, \theta_b^{\kappa+1}]$, $\mathbf{w}_n = [w_n^0, w_n^1 \cdots, w_n^{\kappa+1}]$ and $\boldsymbol{\theta}_n = [\theta_n^0, \theta_n^1 \cdots, \theta_n^{\kappa+1}]$. Eq. (27) can then be discretised into 4κ equations, and the boundary conditions in Eqs. (28) and (29) or (42) can be discretized into eight equations based on four dummy nodes. Finally, we can formulate these discrete equations into a form as $\mathbf{AX} = \mathbf{B}$, where $\mathbf{A} \in \mathbb{R}^{(4\kappa+8)\times(4\kappa+8)}$ is the coefficient matrix, and $\mathbf{B} \in \mathbb{R}^{4\kappa+8}$ is the external force and torque. In our calculations, we set $\kappa = 1000$ to obtain the deformations and load distributions of the bolt-nut connections.

Fig. 7 presents the stress contours of the FE model in a cylindrical coordinate for both the small lead and the large lead cases, in which only external tension was set on the bolt, where $P = 1000$ N and $\Gamma = 0$ Nm. Figs. 7 (a) and (b) show the normal stress σ_{zz} distributions for the small and large cases, respectively. It is seen that the closer to the external load, the greater the magnitude of stress σ_{zz} is, in agreement with the findings in [31, 32]. Comparing the shear stress $\sigma_{z\theta}$ for the small lead case in Fig. 7(c) and for the large lead case in Fig. 7(d), the distribution of the shear stress for the small case is more uniform, while the magnitude of the shear stress for the large lead case is greater as a whole. Using the probe tool of the FEM software, the normal stress σ_{zz} and the shear stress $\sigma_{z\theta}$ over the cross-section of the bolt or nut can be automatically integrated to obtain the tension and torsion of the cross-section.

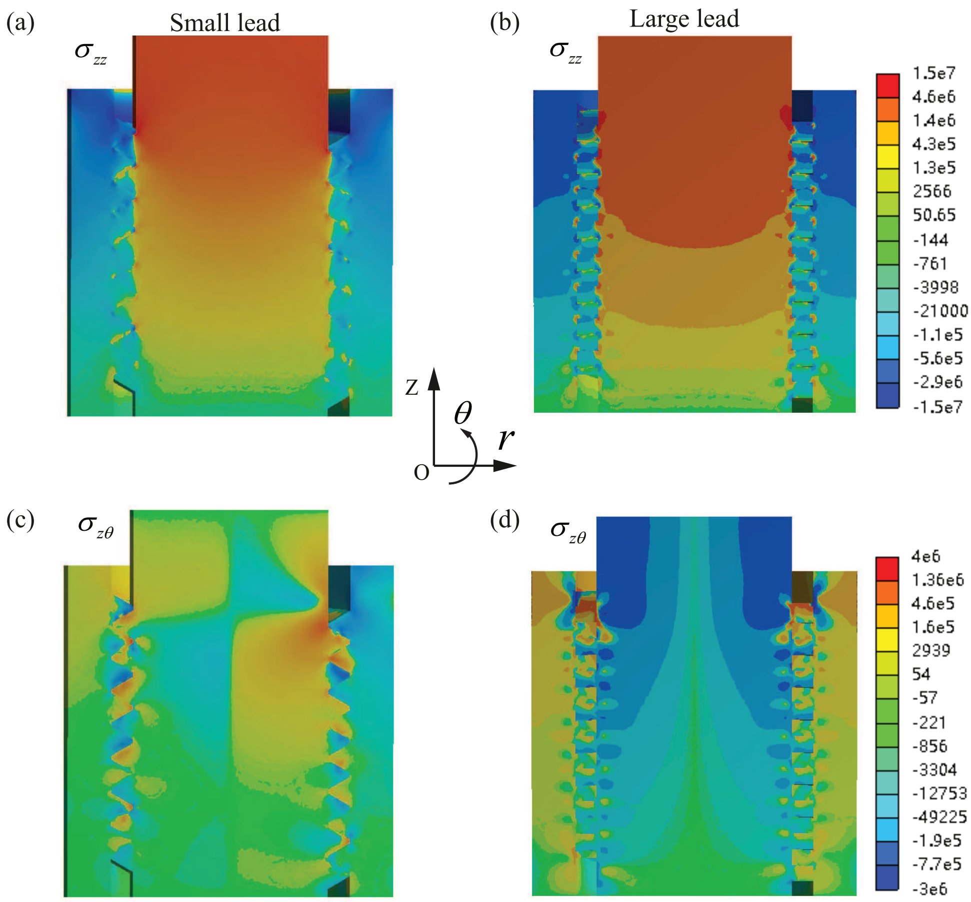

Figure 7: (Colour online) Stress contours of the FE model for (a) the normal stress σ_{zz} of the small lead case, (b) the normal stress σ_{zz} of the large lead case, (c) the shear stress $\sigma_{z\theta}$ of the small lead case and (d) the shear stress $\sigma_{z\theta}$ of the large lead case. Both bolt-nut connections are shown by a one-half cutaway view.

Fig. 8 shows the comparision between the results obtained from the proposed model, the analytical solution and the FE model. Fig. 8(a) displays the distribution of the relative tension for the bolt $\hat{N}_b = N_b/P$ as a function of the relative position $\hat{z} = z/L$. It is seen that the results of the proposed model have a good agreement with the FE results for both the small and large lead cases. For the small lead case, the analytical solutions coincide with the results of the proposed model. For the large lead case, the difference between the numerical and the analytical results is also small. The distributions of the relative torsion for the bolt $\hat{T}_b = T_b/(Pa)$ as a function of the relative position $\hat{z} = z/L$ are presented in Fig. 8(b), which shows a good agreement between the results of the proposed model and the FEM analysis. Figs. 8(c) and (d) present the distributions of the relative tension $\hat{N}_n = N_n/P$ and the relative torsion $\hat{T}_n = T_n/(Pa)$ for the nut as functions of the relative position $\hat{z} = z/L$, respectively. It can be seen that the load distributions of the nut take an opposite sign with that of the bolt. In addition, both the solutions of the proposed model and FEM analysis suggest that the torsion of the small lead case is sufficiently small to be ignorable.

Fig. 9 presents the tension and torsion distributions calculated by the proposed and the FE models for the small lead connection under different external torques, where boundary conditions in Eqs. (28)

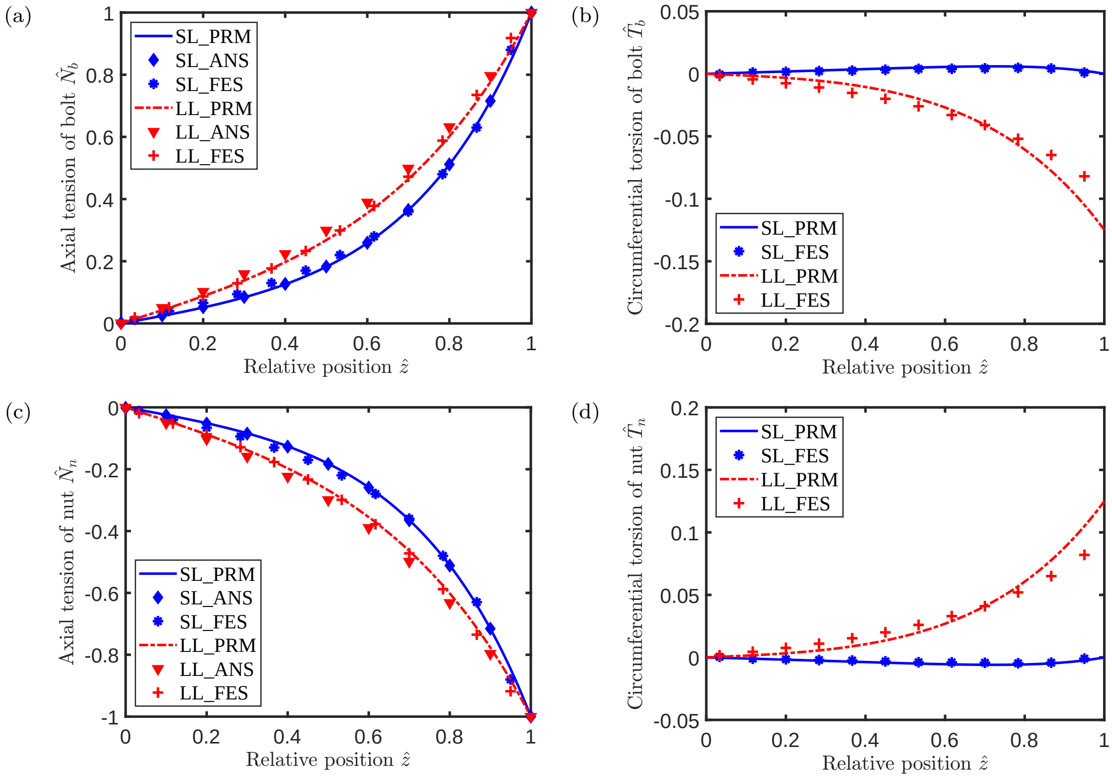

Figure 8: (Colour online) (a) Dimensionless tension $\hat{N}_b$ of the bolt, (b) dimensionless torsion $\hat{T}_b$ of the bolt, (c) dimensionless tension $\hat{N}_n$ of the nut and (d) dimensionless torsion $\hat{T}_n$ of the nut as functions of the relative position $\hat{z} = z/L$ for the small lead (SL) and large lead (LL) cases calculated by using the proposed model (PRM), the analytical solution (ANS) and the finite element solution (FES). It shows a good agreement between the results of the proposed model and the FEM analysis, and it is seen that torsion of the small lead case is sufficiently small to be ignorable.

and (29) were applied. A pre-tension $P = 1000$ N was applied on the bolt at $z = L$, and the torque was set to $\hat{\Gamma} = \Gamma/(Pa) = 0.0,\ -0.5,\ -1.0$ and -1.5 Nm at $z = L$. As can be seen from Fig. 9(a), the torque has very little influence on the tension distribution of the bolt. The result in Fig. 9(b) suggests that the magnitude of the torsion increases as the magnitude of the external torque increases. For both tension and torsion distributions, their numerical results are well consistent with the FE solutions.

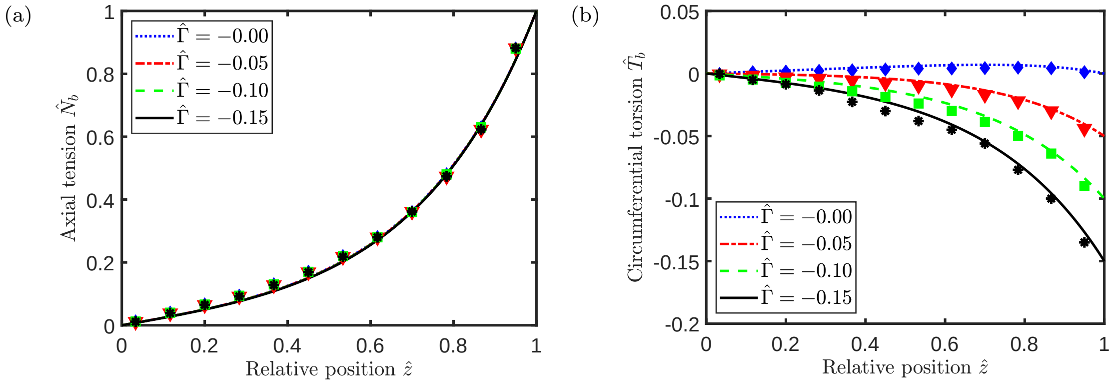

Figure 9: (Colour online) (a) Dimensionless tension $\hat{N}_b$ and (b) dimensionless torsion $\hat{T}_b$ of the bolt as functions of the relative position $\hat{z}$ for external torque $\hat{\Gamma} = \Gamma/(Pa) = 0.0,\ -0.5,\ -1.0$ and -1.5 Nm. The results obtained from the proposed and the FE models are denoted by lines and dots, respectively. As the magnitude of the external torque increases, the magnitude of the torsion increases, but the tension changes a little.

5.3. Influence of physical parameters on load distribution

In this subsection, the influence of the geometrical and material parameters on load distribution in the bolt-nut connection was studied. For the small lead case, there is only one parameter ω in Eq. (34) to be investigated. From Eq. (35), it can be seen that ω is a function of the tensile stiffness of the bolt and nut, the bending thread's stiffness , shape, number and the lead angel.

Fig. 10 presents the dimensionless tension $\hat{N}_b$ and the dimensionless axial contact load $\hat{q} = qL/P$ of the bolt as functions of the relative position $\hat{z}$ under different dimensionless $\hat{\omega} = \omega L$. It can be seen that $\hat{q}$ is the derivative of $\hat{N}_b$ with respect to $\hat{z}$. When the value of ω is small, the tension of the bolt increases linearly as $\hat{z}$ increases, and the distribution of the contact force is uniform along the axial direction. As the value of ω increases, the distribution of the contact force becomes more concentrated in the area where the force is applied ($\hat{z} = 1$).

For the large lead case, the torsion distribution in bolt-nut connection was calculated. The dimensionless circumferential torsion $\hat{T}_b$ and the dimensionless contact torque of the bolt $\hat{\tau} = \tau L/Pa$ as functions of the relative position $\hat{z}$ under different leads are shown in Fig. 11. It is seen that the torsion and the contact torque of the bolt becomes larger at the positions closer to the site of the external force applied. When the lead angle increases, the torsion of the bolt increases as well. So the torsional strength should be taken into consideration in the bolt-nut connection with a large lead.

Fig. 12 displays the effect of ratio of radii between the nut and bolt on the tension and torsion distributions of the bolt-nut connection with a large lead angle. Fig. 12(a) indicates that, as the nut radius increases, the tension load distribution becomes more uniform and tends to a limit curve. Similar phenomenon can be observed from the torsion distribution presented in Fig. 12(b). However, the nut

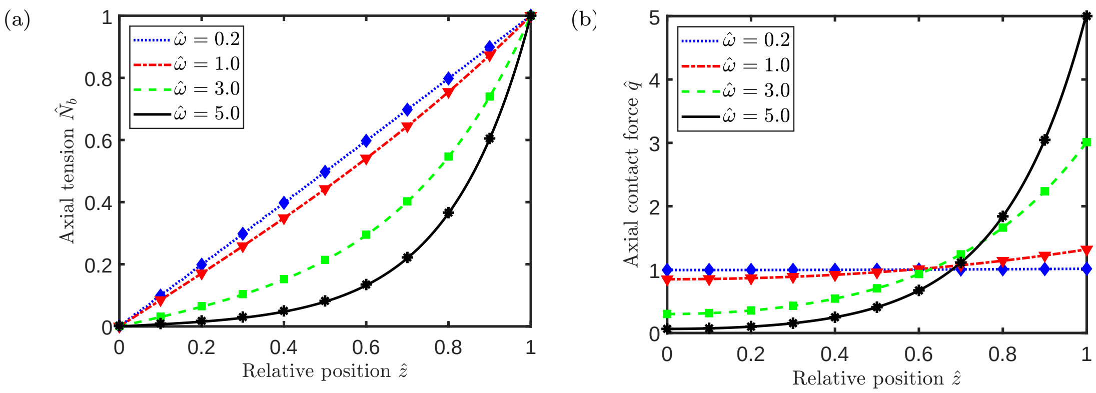

Figure 10: (Colour online) (a) Dimensionless axial tension $\hat{N}_b$ and (b) dimensionless axial contact force $\hat{q}$ of the bolt vary as functions of the relative position $\hat{z}$ calculated for $\hat{\omega} = 0.2$, 1.0, 3.0 and 5.0. Numerical and analytical results are denoted by lines and dots, respectively. As the value of $\hat{\omega}$ increases, the distribution of the contact force becomes more concentrated near the area where the force is applied.

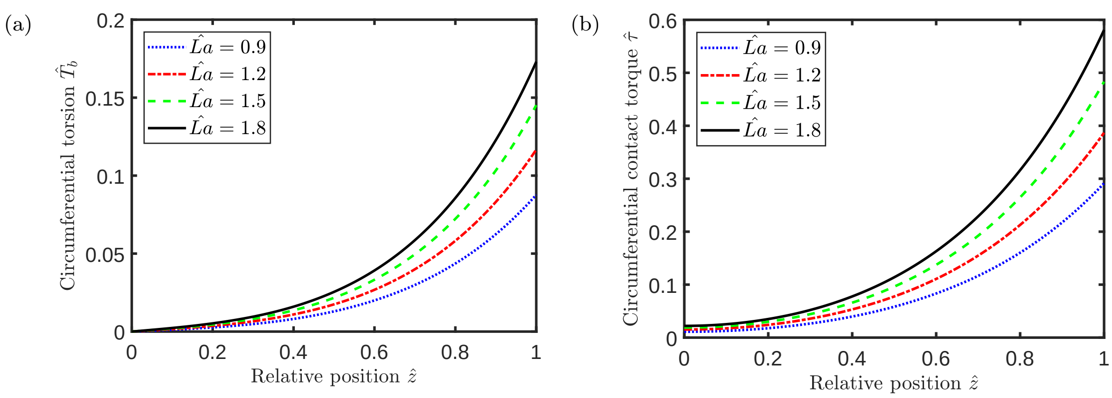

Figure 11: (Colour online) (a) Dimensionless circumferential torsion $\hat{T}_b$ and (b) dimensionless contact torque $\hat{\tau}$ of the bolt vary as functions of the relative position $\hat{z}$ calculated for $\hat{La} = La/a = 0.9$, 1.2, 1.5 and 1.8. It is seen that the torsion of the bolt increases as the lead angle increases.

radius has little influence on the maximum of the torsion. This may shed a light on optimising the torsion distribution by designing the nut with a proper radius.

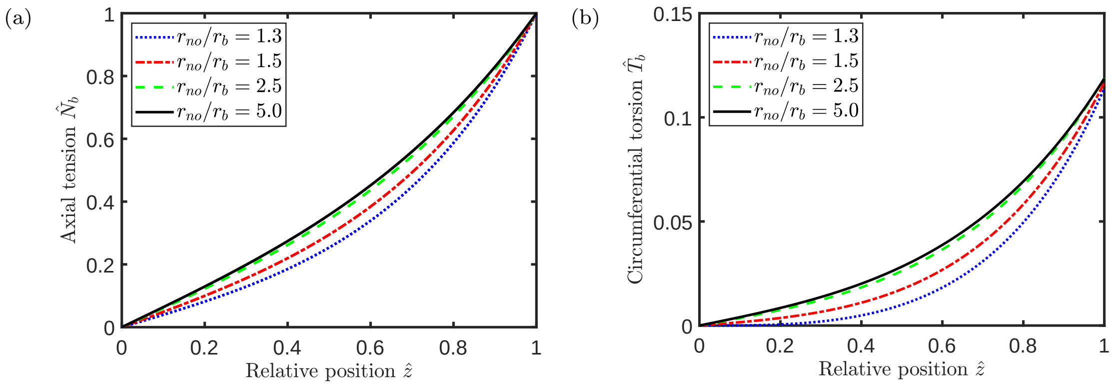

Figure 12: (Colour online) (a) Dimensionless axial tension $\hat{N}_b$, (b) dimensionless circumferential torsion $\hat{T}_b$ of the bolt vary as functions of the relative position $\hat{z}$ calculated for $r_{no}/r_b = 1.3$, 1.5, 2.5 and 5.0. The tension and torsion load distributions become more uniform and tends to a limit curve as the nut radius increases.

6. Concluding remarks

A comprehensive model that can provide the tension and torsion load distributions in a general bolt-nut connection was built up for the first time. Firstly, the thread of the connection was simplified as a classical cantilever beam model to obtain its stiffness. The main structures of the bolt and nut were modelled as homogeneous bars to consider their tension and torsion deformations. Then compatibility conditions for the deformations of the threads and the main structures of the bolt and nut were derived. By using these compatibility conditions, contact force was calculated as a function of tensional and torsional deformations of the bolt and nut. Finally, the tension-torsion coupled governing equations of equilibrium in the axial and circumferential directions was built.

According to the critical sate of Coulomb friction between threads, we obtain a self-locked lead angle responsible for the static balance of threaded connection. For the bolt-nut connection with a lead angle smaller than its self-locked lead angle, the connection can be balanced by friction under pure tension load. In this case, the contact torque is zero and the torsional deformations of the bolt and nut can be neglected. Thus, an analytical model of the tension distribution can be obtained from the tension-torsion coupled model, which coincides with Sopwith's and Yamamoto's models [31, 32]. The analytical solution indicates that the load distribution is only affected by the dimensionless quantity $\hat{\omega} = \omega L$, which is a function of geometrical and material parameters of the bolt-nut connection. When $\hat{\omega}$ is small, the contact load is uniformly distributed along the axial direction. If $\hat{\omega}$ is large, the contact load mainly concentrates on the area where the external axial force is applied.

The proposed model was validated for both small and large lead cases through FEM analysis. The tensions and torsions calculated from the proposed model were in a good agreement with the results from FEM analysis. By using the proposed model, the influence of the geometrical and material parameters on the load distribution in the bolt-nut connection was investigated.

In conclusion, the tension-torsion coupled model for load distribution can provide a theoretical foundation for the design of general bolt-nut connections with different types of leads under various boundary conditions. Future works include the analyses of anti-loosening and dynamical responses of the bolt-nut connection and their experimental validations.

Acknowledgments

This work has been supported by the National Natural Science Foundation of China under Grant Nos.11923001, U2241264.

References

[1] S. Baragetti, A. Terranova, M. Vimercati, Friction behaviour evaluation in berylliumcopper threaded connections, International Journal of Mechanical Sciences 51 (11-12) (2009) 790–796.

[2] H. Yu, Z. Wang, J. Yuan, Loosening and fracture behavior of hybrid titanium-to-steel threaded connection under cyclic loading condition, Engineering Failure Analysis 142 (2022) 106742.

[3] M. Cai, P. Wang, W. Zhang, M. Liu, G. Zhai, F. Z. Liu, Y. Hu, Experimental study on cyclic behavior of thread-fixed one-side bolts bolted endplate connection to strengthened concrete filled square steel tube with fixed thread length, Journal of Building Engineering 60 (2022) 105192.

[4] G. Hao, L. Jianhua, F. Huihua, Review on anti-loosening methods for threaded fasteners, Chinese Journal of Aeronautics 35 (2) (2022) 47–61.

[5] D. Chen, Y. Ma, B. Hou, R. Liu, W. Zhang, Tightening behavior of bolted joint with non-parallel bearing surface, International Journal of Mechanical Sciences 153-154 (2019) 240–253.

[6] H. Gong, J. Liu, X. Ding, Thorough understanding on the mechanism of vibration-induced loosening of threaded fasteners based on modified iwan model, Journal of Sound and Vibration 473 (2020) 115238.

[7] H. Fransplass, M. Langseth, O. Hopperstad, Tensile behaviour of threaded steel fasteners at elevated rates of strain, International journal of mechanical sciences 53 (11) (2011) 946–957.

[8] S. A. Nassar, X. Yang, Novel formulation of the tightening and breakaway torque components in threaded fasteners, Journal of Pressure Vessel Technology 129 (4) (2007) 147–160.

[9] H. Xu, T. Shi, Z. Zhang, B. Shi, Loading and contact stress analysis on the thread teeth in tubing and casing premium threaded connection, Mathematical Problems in Engineering 2014 (2014) 1–11.

[10] J. L. P. Quispe, I. P. Pasqualino, S. F. Estefen, M. I. L. de Souza, Structural behavior of threaded connections for sandwich pipes under make-up torque, external pressure, and axial load, International Journal of Pressure Vessels and Piping 186 (2020) 104156.

[11] I. Argatov, I. Sevostianov, Health monitoring of bolted joints via electrical conductivity measurements, International Journal of Engineering Science 48 (10) (2010) 874–887.

[12] M. Nithyadharan, V. Kalyanaraman, Experimental study of screw connections in CFS-calcium silicate board wall panels, Thin-Walled Structures 49 (6) (2011) 724–731.

[13] K. Yang, Y. Bai, C. Ding, S. Y. Kong, Comparative study on mechanical performance of bolted joints with steel and fibre reinforced polymer bolts, Journal of Building Engineering 41 (2021) 102457.

[14] Y. Q. Wang, W. C. Xing, J. Wang, Q. Chai, Theoretical and experimental studies on vibration characteristics of bolted joint multi-plate structures, International Journal of Mechanical Sciences 252 (2023) 108348.

[15] S. Swensen, G. Deierlein, E. Miranda, Behavior of screw and adhesive connections to gypsum wallboard in wood and cold-formed steel-framed wallettes, Journal of Structural Engineering 142 (4) (2015) E4015002.

[16] H. Hong, H. Lee, N. Jeong, K. Baek, M. Suh, A study on an equivalent model of the threaded fasteners in complex structures through tightening and loosening analysis, Journal of Mechanical Science and Technology 34 (2020) 1195–1205.

[17] S. E. Asnis, J. J. Ernberg, M. P. Bostrom, T. M. Wright, R. M. Harrington, A. Tencer, M. Peterson, Cancellous bone screw thread design and holding power, Journal of Orthopaedic Trauma 10 (7) (1996) 462–469.

[18] F. Younes, A. Eghbali, S. De Troyer, T. De Bruyckere, R. Cleymaet, J. Cosyn, Marginal and apical bone stability after staged sinus floor augmentation using bone condensing implants with variable-thread design: a two-dimensional analysis, International journal of Oral and Maxillofacial Surgery 45 (9) (2016) 1135–1141.

[19] S. Dundar, T. Topkaya, M. Y. Solmaz, F. Yaman, Y. Atalay, A. Saybak, F. Asutay, O. Cakmak, Finite element analysis of the stress distributions in peri-implant bone in modified and standard-threaded dental implants, Biotechnology and Biotechnological Equipment 30 (1) (2016) 127–133.

[20] J. Rys, F. Lisowski, The computational model of the load distribution between elements in a planetary roller screw, Journal of Theoretical and Applied Mechanics 52 (3) (2014) 699–705.

[21] W. Zhou, R. Zhang, S. Ai, R. He, Y. Pei, D. Fang, Load distribution in threads of porous metal–ceramic functionally graded composite joints subjected to thermomechanical loading, Composite Structures 134 (2015) 680–688.

[22] F. Abevi, A. Daidie, M. Chaussumier, M. Sartor, Static load distribution and axial stiffness in a planetary roller screw mechanism, Journal of Mechanical Design 138 (1) (2016) 012301.

[23] S.-i. Nishida, C. Urashima, H. Tamasaki, A new method for fatigue life improvement of screws, European Structural Integrity Society 22 (1997) 215–225.

[24] G. Majzoobi, G. Farrahi, N. Habibi, Experimental evaluation of the effect of thread pitch on fatigue life of bolts, International Journal of Fatigue 27 (2) (2005) 189–196.

[25] N. Sase, S. Koga, K. Nishioka, H. Fujii, Evaluation of anti-loosening nuts for screw fasteners, Journal of Materials Processing Technology 56 (1-4) (1996) 321–332.

[26] A. Bhattacharya, A. Sen, S. Das, An investigation on the anti-loosening characteristics of threaded fasteners under vibratory conditions, Mechanism and Machine Theory 45 (8) (2010) 1215–1225.

[27] B. Kenny, E. Patterson, The distribution of load and stress in the threads of fasteners - A review, Journal of the Mechanical Behavior of Materials 2 (1-2) (1989) 87–106.

[28] A. Mehmanparast, S. Lotfian, S. P. Vipin, A review of challenges and opportunities associated with bolted flange connections in the offshore wind industry, Metals 10 (6) (2020) 732.

[29] J. Huang, J. Liu, H. Gong, X. Deng, A comprehensive review of loosening detection methods for threaded fasteners, Mechanical Systems and Signal Processing 168 (2022) 108652.

[30] J. Den Hartog, The mechanics of plate rotors for turbogenerators, Journal of Applied Mechanics 51 (1929) 1–10.

[31] D. Sopwith, The distribution of load in screw threads, Proceedings of the Institution of Mechanical Engineers 159 (1) (1948) 373–383.

[32] A. Yamamoto, The theory and computation of threads connection, Tokoy: Yokendo, 1980.

[33] S. Lu, D. Hua, Y. Li, F. Cui, P. Li, Stiffness calculation model of thread connection considering friction factors, Mathematical Problems in Engineering 2019 (2019) 1–19.

[34] J. Goodier, The distribution of load on the threads of screws, Trans. ASME, Journal of Applied Mechanics 62 (1940) 10–16.

[35] B. Kenny, E. Patterson, Load and stress distribution in screw threads, Experimental Mechanics 25 (3) (1985) 208–213.

[36] E. Patterson, B. Kenny, A modification to the theory for the load distribution in conventional nuts and bolts, The Journal of Strain Analysis for Engineering Design 21 (1) (1986) 17–23.

[37] H. Chen, P. Zeng, G. Fang, L. Lei, Load distribution of bolted joint, Chinese Journal of Mechanical Engineering 46 (9) (2010) 171–178.

[38] J.-P. Geng, K. B. Tan, G.-R. Liu, Application of finite element analysis in implant dentistry: a review of the literature, The Journal of prosthetic dentistry 85 (6) (2001) 585–598.

[39] J. Mackerle, Finite element analysis of fastening and joining: A bibliography (1990–2002), International Journal of Pressure Vessels and Piping 80 (4) (2003) 253–271.

[40] H. Zhang, L. Zhang, Z. Liu, S. Qi, Y. Zhu, P. Zhu, Numerical analysis of hybrid (bonded/bolted) frp composite joints: A review, Composite Structures 262 (2021) 113606.

[41] G. Yang, J. Hong, L. Zhu, B. Li, M. Xiong, F. Wang, Three-dimensional finite element analysis of the mechanical properties of helical thread connection, Chinese Journal of mechanical engineering 26 (3) (2013) 564–572.

[42] Maruyama, Kazuo, Stress analysis of a bolt-nut joint by the finite element method and copper-electroplating method : 3rd report, influence of pitch error or flank angle error, Transactions of the Japan Society of Mechanical Engineers 41 (348) (1975) 2292–2302.

[43] K. Maruyama, Stress analysis of a bolt-nut joint by the finite element method and the copper-electroplating method : 1st report, stress at the root of a v-grooved rod under a tensile load, Transactions of the Japan Society of Mechanical Engineers 38 (312) (1972) 1975–1981.

[44] Kazuo, Maruyama, Stress analysis of a bolt-nut joint by the finite element method and the copper-electroplating method : 2nd report, stress at the root of a bolt thread under a tensile load, Transactions of the Japan Society of Mechanical Engineers 39 (324) (1973) 2340–2349.

[45] J. L. Bretl, R. D. Cook, Modelling the load transfer in threaded connections by the finite element method, International Journal for Numerical Methods in Engineering 14 (9) (1979) 1359–1377.

[46] D. J. Segalman, M. J. Starr, Modeling of threaded joints using anisotropic elastic continua, Journal of Applied Mechanics 74 (2007) 575–585.

[47] N. Motosh, Load distribution on threads of titanium tension nuts and steel bolts, Journal of Engineering for Industry 97 (1) (1975) 162–166.

[48] W. Wang, K. Marshek, Determination of load distribution in a threaded connector with yielding threads, Mechanism and Machine Theory 31 (2) (1996) 229–244.

[49] H. Zhao, A numerical method for load distribution in threaded connections, Journal of Mechanical Design 118 (2) (1996) 274–279.

[50] T. Fukuoka, N. Yamasaki, H. Kitagawa, M. Hamada, A stress analysis of threaded portions in fastening, Transactions of the Japan Society of Mechanical Engineers 28 (244) (1985) 2247–2253.

[51] T. Fukuoka, T. Takaki, Elastic plastic finite element analysis of bolted joint during tightening process, Journal of Mechanical Design 125 (4) (2003) 823–830.

[52] O. Onysko, V. Kopei, I. Medvid, L. Pituley, T. Lukan, Influence of the thread profile accuracy on contact pressure in oil and gas pipes connectors, Lecture Notes in Mechanical Engineering (2020) 432–441.

[53] A. G. Kazantsev, O. M. Petrov, Influence of the accumulated error in thread pitch on the stressstrain state and cyclic strength of threaded joints, Inorganic Materials 51 (15) (2015) 1490–1495.

[54] J. Domblesky, F. Feng, Two-dimensional and three-dimensional finite element models of external thread rolling, Proceedings of the Institution of Mechanical Engineers, Part B: Journal of Engineering Manufacture 216 (4) (2002) 507–517.

[55] C. Xin, N. Nao-Aki, W. M. Abdel, A. Yu-Ichiro, S. Yoshikazu, T. Yasushi, F. Gusztav, Fatigue failure analysis for bolt-nut connections having slight pitch differences using experimental and finite element methods, Acta Polytechnica Hungarica 12 (8) (2015) 61–79.

[56] T. Fukuoka, M. Nomura, Proposition of helical thread modeling with accurate geometry and finite element analysis, Journal of Pressure Vessel Technology 130 (1) (2008) 135–140.

[57] Y. Jiang, M. Zhang, C.-H. Lee, A study of early stage self-loosening of bolted joints, Journal of Mechanical Design 125 (3) (2003) 518–526.

[58] S. Izumi, T. Yokoyama, A. Iwasaki, S. Sakai, Three-dimensional finite element analysis of tightening and loosening mechanism of threaded fastener, Engineering Failure Analysis 12 (4) (2005) 604–615.

[59] N. A. Noda, X. Liu, Y. Sano, K. Tateishi, B. Wang, Y. Takase, Three-dimensional finite element analysis for prevailing torque of bolt-nut connection having slight pitch difference, Journal of Mechanical Science and Technology 34 (6) (2020) 2469–2476.

[60] M. Zhang, D. Zeng, L. Lu, Y. Zhang, J. Wang, J. Xu, Finite element modelling and experimental validation of bolt loosening due to thread wear under transverse cyclic loading, Engineering Failure Analysis 104 (2019) 341–353.

[61] K. Guo, T. Zhang, H. Yuan, Experimental and computational investigations of nonlinear frictional behavior in threaded fasteners, Tribology International 154 (2021) 106737.

[62] X. Liu, J. Fan, H. Wang, J. Jiang, J. Liu, X. Gong, J. Peng, M. Zhu, Effect of wear between contact surfaces on self-loosening behaviour of bolted joint under low frequency torsional excitation, Tribology International 174 (2022) 107764.

[63] F. Mathurin, J. Guillot, P. Stéphan, A. Daidié, 3D finite element modeling of an assembly process with thread forming screw, Journal of Manufacturing Science and Engineering 131 (4) (2009) 041015.

[64] S. Tanaka, Y. Yoshitomi, Analysis of deformation behavior of bolted joint during fastening process, Transactions of the Japan Society of Mechanical Engineers 78 (794) (2012) 3615–3629.

[65] R. Verwaerde, P.-A. Guidault, P.-A. Boucard, A non-linear finite element connector model with friction and plasticity for the simulation of bolted assemblies, Finite Elements in Analysis and Design 195 (2021) 103586.

[66] H. Kumano, T. Sawa, T. Hirose, Mechanical behavior of bolted joints under steady heat conduction, Journal of Pressure Vessel Technology 116 (1) (1994) 42–48.

[67] G. Yuan, Z. Yao, Q. Wang, Z. Tang, Numerical and experimental distribution of temperature and stress fields in api round threaded connection, Engineering Failure Analysis 13 (8) (2006) 1275–1284.

[68] Y. Shoji, T. Sawa, Self-loosening mechanism of nuts due to cyclic thermal load, ASME 2009 Pressure Vessels and Piping Conference 2 (2009) 99–105.

[69] N. A. Noda, X. Liu, Y. Sano, K. Tateishi, B. Wang, Y. Takase, Three-dimensional finite element analysis for prevailing torque of bolt-nut connection having slight pitch difference, Journal of Mechanical Science and Technology 34 (6) (2020) 2469–2476.

[70] M. J. Lee, Y. K. Lee, H. U. Oh, Performance evaluation of hinge driving separation nut-type holding and releasing mechanism triggered by nichrome burn wire, International Journal of Aeronautical and Space Sciences 16 (4) (2015) 602–613.

[71] X. Wang, Z. Qin, J. Ding, F. Chu, Finite element modeling and pyroshock response analysis of separation nuts, Aerospace Science and Technology 68 (9) (2017) 380–390.

[72] F. Foti, L. Martinelli, Mechanical modeling of metallic strands subjected to tension, torsion and bending, International Journal of Solids and Structures 91 (2016) 1–17.

[73] L. Xiang, H. Wang, Y. Chen, Y. Guan, Y. Wang, L. Dai, Modeling of multi-strand wire ropes subjected to axial tension and torsion loads, International Journal of Solids and Structures 58 (2015) 233–246.

[74] Z. Zhao, C. Liu, W. Ma, Characteristics of steady vibration in a rotating hub–beam system, Journal of Sound and Vibration 363 (2016) 571–583.

[75] N. Wang, T. Shi, C. Liu, Analysis for the free vibration of rotating variablecross-section beam, Scientia Sinica Physica, Mechanica and Astronomica 49 (2) (2019) 024511.